International Journal of Thermal Sciences 49 (2010) 1856–1865

Contents lists available at ScienceDirect

International Journal of Thermal Sciences

journal homepage: www.elsevier.com/locate/ijts

Effect of magnetic field on natural convection flow in a liquid gallium filled square cavity for linearly heated side wall(s)

M. Sathiyamoorthy [a], Ali Chamkha [b,*]

[a] Department of Mathematics, SSN College of Engineering, Kalavakkam, Chennai 603110, India
[b] Manufacturing Engineering Department, The Public Authority for Applied Education and Training, P.O. Box 42325, Shuweikh 70654, Kuwait

ARTICLE INFO

Article history:
Received 13 June 2009
Received in revised form
23 March 2010
Accepted 19 April 2010
Available online 23 May 2010

Keywords:
Penalty finite element method
MHD convective flow
Square cavity
Liquid metals
Non-uniform heating

ABSTRACT

A numerical study is presented for natural convection flow of electrically conducting liquid gallium in a square cavity. In the cavity, the bottom wall is uniformly heated and the left vertical wall is linearly heated whereas the right vertical wall is linearly heated or cooled while the top wall kept thermally insulated. A uniform magnetic field inclined at an angle ϕ with respect to horizontal plane is externally imposed. Penalty finite element method with bi-quadratic rectangular elements is used to solve the non-dimensional governing equations. Numerical results are presented for wide range of Hartmann number ($Ha = 0$–100) with inclined angles ($\phi = 0, \pi/2$) for high Rayleigh number $Ra = 10^5$ in terms of stream functions and isotherm contours, local and average Nusselt number. The results shows that the magnetic field with inclined angle has effects on the flow and heat transfer rates in the cavity. It is also found that the average Nusselt number decreases non-linearly by increasing Hartmann number for any inclined angle.

© 2010 Elsevier Masson SAS. All rights reserved.

1. Introduction

The phenomenon of natural convection in enclosures is not new problem for research. A rich and variety of numerical results have been published for last three decades due to this phenomenon often affects the thermal performance in many engineering and science applications such as boilers, nuclear reactor systems, energy storage and conservation, fire control and chemical, food and metallurgical industries. In this context natural convection of an electrically conducting fluid in a magnetic field have been studied in resent years by several authors. Because the process of manufacturing materials in industrial problems and microelectronic heat transfer devices involve an electrically conducting fluid subjected to magnetic field. In this case the fluid experiences a Lorentz force and its effect is to reduce the flow velocities which turn the affects in the heat transfer rate. A comprehensive literature survey concerned with this subject is given by Yang [1], Kulacki et al. [2], Moreau [3], Utech and Flemmings [4], Vives and Perry [5] and Series and Hurle [6].

Among the earlier studies, it may be noted that Ozoe and Maruo [7], Ozoe and Okada [8], Garandet et al. [9] and Venkatachalappa and Subbaraya [10] have made attempts to acquire a basic understanding of flows and heat transfer characteristics in an enclosure in the presence of magnetic field. They found that the magnetic field decreases the heat transfer rate. Rudraiah et al. [11] and Alchaar et al. [12] have shown a specific interest to focus on a natural convection within a rectangular enclosure with a magnetic field where one vertical wall is cooled and another one heated while the remaining top and bottom walls are well insulated. Recently, Ece and Buyuk [13] illustrated the natural convection flow under a magnetic field in a inclined rectangular cavity for heated and cooled on the adjacent walls. Mahmud and Fraser [14] have investigated magnetohydrodynamic natural convection flow and entropy generation in a square cavity. On the contrary Grosan et al. [15] has studied effects of magnetic field and internal heat generation on natural convection flow in rectangular cavity filled with porous medium. In most of the previous studies, isothermal or isoflux thermal boundary conditions were applied to side walls of enclosures. However, the influence of non-isothermal boundary conditions in natural convection flow in enclosures without magnetic field has been studied by several authors (Sarris et al. [16], Roy and Basak [17], Basak et al. [18] and Bilgen and Ben Yedder [19]).

The present paper investigates the effect of magnetic field on natural convection flow within a square cavity filled with an electrically conducting liquid gallium when the bottom wall is heated uniformly, left vertical wall is linearly heated and right vertical wall is linearly heated or cooled while the top wall is well insulated. The same problems has been studied without magnetic field by the authors [20] who have reported natural convection flow in a square

* Corresponding author.
E-mail addresses: m.sathiya@yahoo.com (M. Sathiyamoorthy), achamkha@yahoo.com (A. Chamkha).

1290-0729/$ – see front matter © 2010 Elsevier Masson SAS. All rights reserved.
doi:10.1016/j.ijthermalsci.2010.04.014

cavity for the same boundary conditions as considered in this work. In linearly heated side walls system, four recirculating symmetrical cells are formed in the cavity and two recirculating cells are formed for cooled at right wall with $Ra = 10^5$. The main object is to determine the influence of Hartmann number with inclined angles on deformation of the recirculating cells, temperature distributions within the cavity and heat transfer rates at the heated walls in terms of Nusselt numbers. In the current study, Galerkin finite element method with penalty parameter has been used to solve the non-linear coupled partial differential equations for flow and temperature field.

2. Mathematical formulation

Consider a square cavity filled with viscous, incompressible and electrically conducting fluid which is permeated by a uniform magnetic field $\overline{B}$ with magnitude B at an inclined angle ϕ from the horizontal plane (Fig. 1). The Boussinesq approximation is invoked for the fluid properties to relate density changes to temperature changes. The viscous, radiation and Joule heating effects are neglected. The magnetic Reynolds number is assumed to be small so that the induced magnetic field is neglected.

Under the above assumption, the conservation equations for momentum and electric transfer are given by

$$(\overline{V}\cdot\nabla)\overline{V} = -\frac{1}{\rho}\nabla p + \nu\nabla^2\overline{V} + \frac{\overline{J}}{\rho}\times\overline{B} - \beta(T-Tc)\overline{g} \tag{1}$$

$$\overline{J} = \sigma(-\nabla\varphi + \overline{V}\times\overline{B}) \tag{2}$$

$$\nabla^2\overline{\varphi} = \overline{B}\cdot\omega,\ \omega = \nabla\times\overline{V} \tag{3}$$

where $\overline{V}$ is the fluid velocity vector, ω is vorticity field, T is the fluid temperature, p is pressure, $\overline{B}$ is the external magnetic field, $\overline{J}$ is the electric current, φ is the electric potential, σ is electric conductivity and $-\nabla\varphi$ is associated electric field. As discussed by Sreenivasan et al. [21] for the case of a steady and two-dimensional flow where the magnetic field lies in the plane of motion, Eqns. (3) reduces to $\nabla^2\varphi = 0$, and provided the fluid is bounded by perfectly conducting walls that provide a resistance-free path from induced current. It follows that the electric field vanishes everywhere in the cavity. Under these conditions the usual two-dimensional governing equations for the steady natural convection flow using conservation of mass, momentum and energy can be written as

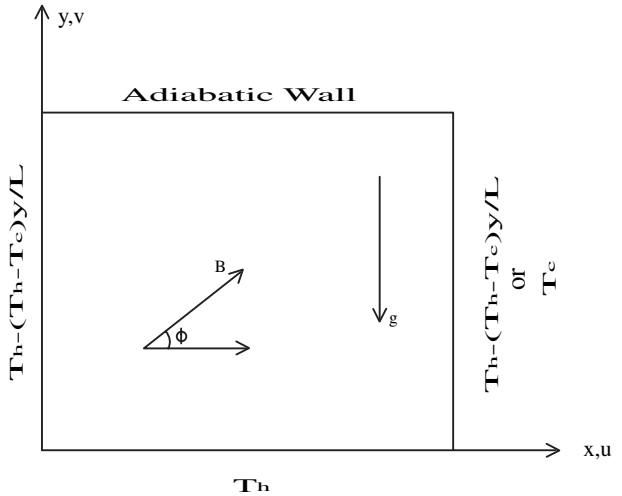

Fig. 1. Schematic diagram of the physical system.

$$\frac{\partial u}{\partial x} + \frac{\partial v}{\partial y} = 0 \tag{4}$$

$$u\frac{\partial u}{\partial x} + v\frac{\partial u}{\partial y} = -\frac{1}{\rho}\frac{\partial p}{\partial x} + \nu\left(\frac{\partial^2 u}{\partial x^2} + \frac{\partial^2 u}{\partial y^2}\right) + \frac{\sigma B^2}{\rho}\left(v\sin\phi\cos\phi - u\sin^2\phi\right) \tag{5}$$

$$u\frac{\partial v}{\partial x} + v\frac{\partial v}{\partial y} = -\frac{1}{\rho}\frac{\partial p}{\partial y} + \nu\left(\frac{\partial^2 v}{\partial x^2} + \frac{\partial^2 v}{\partial y^2}\right) + g\beta(T-T_c) + \frac{\sigma B^2}{\rho}\left(u\sin\phi\cos\phi - v\cos^2\phi\right) \tag{6}$$

$$u\frac{\partial T}{\partial x} + v\frac{\partial T}{\partial y} = \alpha\left(\frac{\partial^2 T}{\partial x^2} + \frac{\partial^2 T}{\partial y^2}\right) \tag{7}$$

with boundary conditions

$$\begin{aligned} &u(x,0) = u(x,L) = u(0,y) = u(L,y) = 0,\\ &v(x,0) = v(x,L) = v(0,y) = v(L,y) = 0,\\ &T(x,0) = T_h, \frac{\partial T}{\partial y}(x,L) = 0, 0 < x < L,\\ &T(0,y) = T_h - (T_h - T_c)\frac{y}{L}, T(L,y) = T_h - (T_h - T_c)\frac{y}{L} \text{ or } T_c. \end{aligned} \tag{8}$$

Using the following change of variables (Fig. 1),

$$X = \frac{x}{L},\ Y = \frac{y}{L},\ U = \frac{uL}{\alpha},\ V = \frac{vL}{\alpha},\ \theta = \frac{T-T_c}{T_h-T_c},\ P = \frac{pL^2}{\rho\alpha^2},$$
$$Pr = \frac{\nu}{\alpha},\ Ra = \frac{g\beta(T_h-T_c)L^3Pr}{\nu^2},\ Ha = LB\sqrt{\frac{\sigma}{\mu}} \tag{9}$$

The governing equations (4)–(7) reduce to non-dimensional form as:

$$\frac{\partial U}{\partial X} + \frac{\partial V}{\partial Y} = 0 \tag{10}$$

$$U\frac{\partial U}{\partial X} + V\frac{\partial U}{\partial Y} = -\frac{\partial P}{\partial X} + Pr\left(\frac{\partial^2 U}{\partial X^2} + \frac{\partial^2 U}{\partial Y^2}\right) + PrHa^2\left(V\ \sin\ \phi\ \cos\ \phi - U\ \sin^2\ \phi\right) \tag{11}$$

$$U\frac{\partial V}{\partial X} + V\frac{\partial V}{\partial Y} = -\frac{\partial P}{\partial Y} + Pr\left(\frac{\partial^2 V}{\partial X^2} + \frac{\partial^2 V}{\partial Y^2}\right) + RaPr\theta + PrHa^2\left(U\ \sin\phi\cos\phi - V\cos^2\phi\right) \tag{12}$$

$$U\frac{\partial\theta}{\partial X} + V\frac{\partial\theta}{\partial Y} = \left(\frac{\partial^2\theta}{\partial X^2} + \frac{\partial^2\theta}{\partial Y^2}\right) \tag{13}$$

with the boundary conditions

$$\begin{aligned} &U(X,0) = U(X,1) = U(0,Y) = U(1,Y) = 0,\\ &V(X,0) = V(X,1) = V(0,Y) = V(1,Y) = 0,\\ &\theta(X,0) = 1,\ \frac{\partial\theta}{\partial Y}(X,1) = 0,\\ &\theta(0,Y) = 1-Y,\ \theta(1,Y) = 1-Y \text{ or } 0. \end{aligned} \tag{14}$$

Here X and Y are dimensionless coordinates varying along horizontal and vertical directions, respectively; U and V are, dimensionless velocity components in the X- and Y-directions, respectively; θ is the dimensionless temperature; P is the dimensionless pressure; Ra, Pr, Ha are Rayleigh, Prandtl and Hartmann numbers, respectively.

3. Numerical method and validation

The momentum and energy balance equations (11)–(13) are solved using the Galerkin finite element method. The continuity equation (10) will be used as a constraint due to mass conservation and this constraint may be used to obtain the pressure distribution [22]. In order to solve equations (11)–(13), we use the penalty finite element method where the pressure P is eliminated by a penalty parameter γ and the incompressibility criteria given in equation (10) (see Reddy [22]) which results in

$$P = -\gamma\left(\frac{\partial U}{\partial X}+\frac{\partial V}{\partial Y}\right) \tag{15}$$

The continuity equation (10) is automatically satisfied for large value of γ. A typical value of γ that yields consistent solutions is 10^7 [22].

Using equations (15), the momentum balance equations (11) and (12) reduce to

$$U\frac{\partial U}{\partial X}+V\frac{\partial U}{\partial Y} = \gamma\frac{\partial}{\partial X}\left(\frac{\partial U}{\partial X}+\frac{\partial V}{\partial Y}\right)+Pr\left(\frac{\partial^2 U}{\partial X^2}+\frac{\partial^2 U}{\partial Y^2}\right) + PrHa^2\left(V\sin\phi\cos\phi - U\sin^2\phi\right) \tag{16}$$

and

$$U\frac{\partial V}{\partial X}+V\frac{\partial V}{\partial Y} = \gamma\frac{\partial}{\partial Y}\left(\frac{\partial U}{\partial X}+\frac{\partial V}{\partial Y}\right)+Pr\left(\frac{\partial^2 V}{\partial X^2}+\frac{\partial^2 V}{\partial Y^2}\right) + RaPr\theta + PrHa^2\left(U\sin\phi\cos\phi - V\cos^2\phi\right) \tag{17}$$

Expanding the velocity components (U, V) and temperature (θ) using basis set $\{\Phi_k\}_{k=1}{}^N$ as,

$$U\simeq\sum_{k=1}^{N}U_k\Phi_k(X,Y),\quad V\simeq\sum_{k=1}^{N}V_k\Phi_k(X,Y),\quad \theta\simeq\sum_{k=1}^{N}\theta_k\Phi_k(X,Y). \tag{18}$$

For $0\le X, Y\le 1$, the Galerkin finite element method yields the following non-linear residual equations for equations (13), (16) and (17) respectively, at the nodes $i(1\le i\le N)$ of internal domain Ω:

$$\begin{aligned}R_i^{(1)} &= \sum_{k=1}^{N}U_k\int_\Omega\left[\left(\sum_{k=1}^{N}U_k\Phi_k\right)\frac{\partial\Phi_k}{\partial X}+\left(\sum_{k=1}^{N}V_k\Phi_k\right)\frac{\partial\Phi_k}{\partial Y}\right]\Phi_i dXdY\\ &+\gamma\left[\sum_{k=1}^{N}U_k\int_\Omega\frac{\partial\Phi_i}{\partial X}\frac{\partial\Phi_k}{\partial X}dXdY+\sum_{k=1}^{N}V_k\int_\Omega\frac{\partial\Phi_i}{\partial X}\frac{\partial\Phi_k}{\partial Y}dXdY\right]\\ &+Pr\sum_{k=1}^{N}U_k\int_\Omega\left[\frac{\partial\Phi_i}{\partial X}\frac{\partial\Phi_k}{\partial X}+\frac{\partial\Phi_i}{\partial Y}\frac{\partial\Phi_k}{\partial Y}\right]dXdY-PrHa^2\\ &\int_\Omega\left[\left(\sum_{k=1}^{N}V_k\Phi_k\right)\sin\phi\cos\phi-\left(\sum_{k=1}^{N}U_k\Phi_k\right)\sin^2\phi\right]\\ &\times\Phi_i dXdY\end{aligned} \tag{19}$$

$$\begin{aligned}R_i^{(2)} &= \sum_{k=1}^{N}V_k\int_\Omega\left[\left(\sum_{k=1}^{N}U_k\Phi_k\right)\frac{\partial\Phi_k}{\partial X}+\left(\sum_{k=1}^{N}V_k\Phi_k\right)\frac{\partial\Phi_k}{\partial Y}\right]\Phi_i dXdY\\ &+\gamma\left[\sum_{k=1}^{N}U_k\int_\Omega\frac{\partial\Phi_i}{\partial Y}\frac{\partial\Phi_k}{\partial X}dXdY+\sum_{k=1}^{N}V_k\int_\Omega\frac{\partial\Phi_i}{\partial Y}\frac{\partial\Phi_k}{\partial Y}dXdY\right]\\ &+Pr\sum_{k=1}^{N}V_k\int_\Omega\left[\frac{\partial\Phi_i}{\partial X}\frac{\partial\Phi_k}{\partial X}+\frac{\partial\Phi_i}{\partial Y}\frac{\partial\Phi_k}{\partial Y}\right]dXdY-PrHa^2\\ &\int_\Omega\left[\left(\sum_{k=1}^{N}U_k\Phi_k\right)\sin\phi\cos\phi-\left(\sum_{k=1}^{N}V_k\Phi_k\right)\cos^2\phi\right]\\ &\times\Phi_i dXdY-RaPr\int_\Omega\left(\sum_{k=1}^{N}\theta_k\Phi_k\right)\Phi_i dXdY\end{aligned} \tag{20}$$

$$\begin{aligned}R_i^{(3)} &= \sum_{k=1}^{N}\theta_k\int_\Omega\left[\left(\sum_{k=1}^{N}U_k\Phi_k\right)\frac{\partial\Phi_k}{\partial X}+\left(\sum_{k=1}^{N}V_k\Phi_k\right)\frac{\partial\Phi_k}{\partial Y}\right]\Phi_i dXdY\\ &+\sum_{k=1}^{N}\theta_k\int_\Omega\left[\frac{\partial\Phi_i}{\partial X}\frac{\partial\Phi_k}{\partial X}+\frac{\partial\Phi_i}{\partial Y}\frac{\partial\Phi_k}{\partial Y}\right]dXdY\end{aligned} \tag{21}$$

where

$$\begin{aligned}R_i^{(1)} &= Pr\oint_\Gamma\left(n_X\frac{\partial U}{\partial X}+n_Y\frac{\partial U}{\partial Y}\right)\Phi_i ds,\\ R_i^{(2)} &= Pr\oint_\Gamma\left(n_X\frac{\partial V}{\partial X}+n_Y\frac{\partial V}{\partial Y}\right)\Phi_i ds,\\ R_i^{(3)} &= \oint_\Gamma\left(n_X\frac{\partial\theta}{\partial X}+n_Y\frac{\partial\theta}{\partial Y}\right)\Phi_i ds.\end{aligned}$$

The set of non-linear algebraic equations (19)–(21) are solved using reduced integration technique [22] and Newton–Raphson method. The numerical solutions are obtained in terms of velocity components (U, V) and the stream function (ψ) is evaluated using the relationship between the stream function (ψ) and velocity components [23]. It may be noted that the positive sign of ψ denotes anti-clockwise circulation and the clockwise circulation is represented by the negative sign of ψ. The no-slip condition is valid at all boundaries as there is no cross flow, hence $\psi = 0$ is used for the boundaries.

The heat transfer coefficient in terms of the local Nusselt number is defined by

$$Nu = -\frac{\partial\theta}{\partial n} \tag{22}$$

where n-denotes the normal direction on a plane. The local Nusselt number at bottom wall (Nu_b) and at the side wall (Nu_s) are evaluated for various wall boundary conditions using the above definition. The average Nusselt numbers at the bottom and side walls are computed as follows:

$$\overline{Nu_b} = \int_0^1 Nu_b dX \text{ and } \overline{Nu_s} = \int_0^1 Nu_s dY \tag{23}$$

The computational domain consists of 20×20 bi-quadratic elements which correspond to 41×41 grid points. In order to verify the accuracy of the numerical procedure we have compared the obtained results for the case when magnetic field absent ($Ha = 0$) with benchmark solution of Mallinson and Vahl Davis [24]. Further,

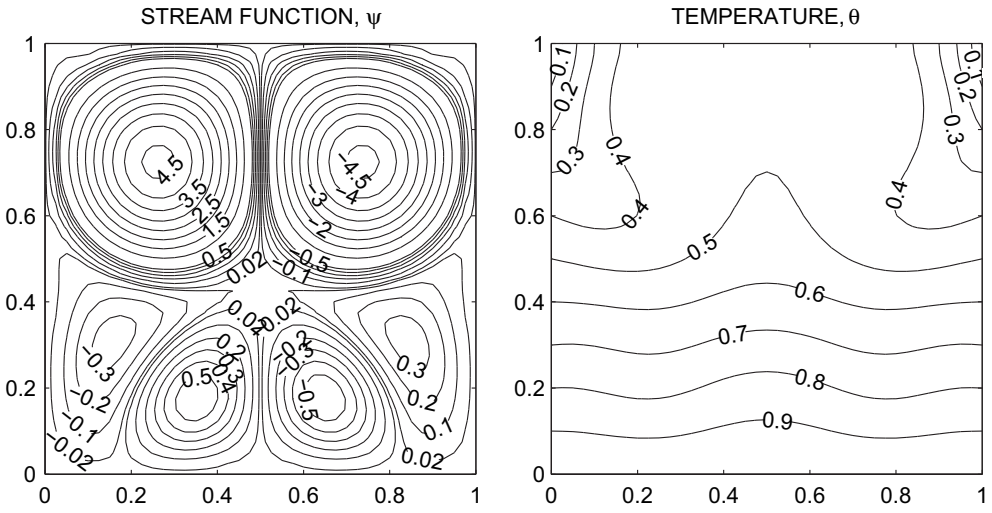

Fig. 2. Contour plots of $\theta(0, Y) = \theta(1, Y) = 1 - Y$ for $Ha = 0$ ($Pr = 0.025$ and $Ra = 10^5$).

a second test concerned with magnetic field which has been investigated by Venkatachalappa and Subbaraya [10]. The agreement was very satisfactory with less than 2 percent deviations for all cases. Computations have been carried out for various values of $Ha = 0$–100 and $\phi = 0, \pi/2$ for $Ra = 10^5$ and $Pr = 0.025$ (liquid gallium) with uniformly heated bottom wall, linearly heated left vertical wall and linearly heated or cooled right vertical wall where the top wall is well insulated.

4. Results and discussions

4.1. Effects of Hartmann number and inclined angle

4.1.1. Case I: linearly heated side walls

In this section, representative results for the streamlines and isotherms for two different magnetic field orientations, horizontally-applied ($\phi = 0$) and vertically-applied ($\phi = \pi/2$) magnetic fields, are presented in Figs. 2–6 for the case of linearly heated vertical walls and the uniformly heated bottom wall of the enclosure.

Figs. 2–4 display steady-state contour maps for the streamline and temperature for values of the Hartmann number Ha (0, 20 and 50) for $Pr = 0.025$, $Ra = 10^5$ and $\phi = 0$(non-inclined magnetic field), respectively. It is clear that the flow within the cavity takes place by virtue of thermal buoyancy effects (caused by the linearly heated walls) which is represented by the Rayleigh number Ra. As seen in Fig. 2 for the relatively high Rayleigh number $Ra = 10^5$ and in the absence of the magnetic field ($Ha = 0$), the flow is characterized by a multi-cellular behavior in which six recirculating cells or eddies of relatively high velocity are formed within the cavity. The three cells that occur at upper left, lower right side and lower left of center are circulating in the anti-clockwise direction and the other three are circulating in the clockwise direction. The stronger cells are formed close to the adiabatic wall of the cavity. Due to the use of same boundary conditions for the left and right walls of the enclosure, the three pairs of cells close to each of the linearly heated walls are symmetric. As expected, because of the boundary-layer effects, the temperature field is characterized by sharp drop in its value near the adiabatic wall of the enclosure while it increases away from it reaching its maximum at the bottom wall. Also, the temperature contour maps are not horizontally uniform in the core region of the enclosure. The application of a transverse magnetic field in the direction normal to the vertical walls ($\phi = 0$) has the tendency to slow down the movement of the fluid in the enclosure (see Fig. 3). As a result, the recirculating cells tend to be stretched or elongated

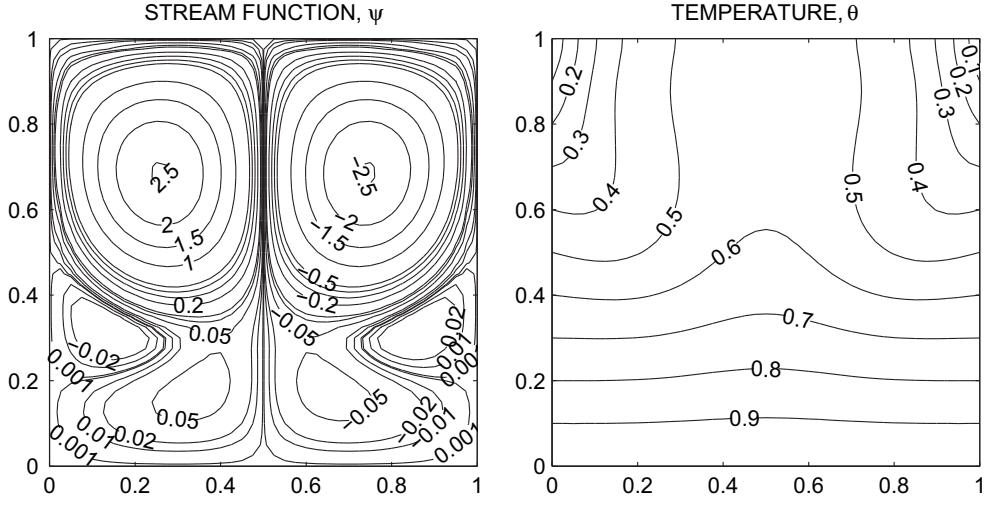

Fig. 3. Contour plots of $\theta(0, Y) = \theta(1, Y) = 1 - Y$ for $Ha = 20$ and $\phi = 0$ ($Pr = 0.025$ and $Ra = 10^5$).

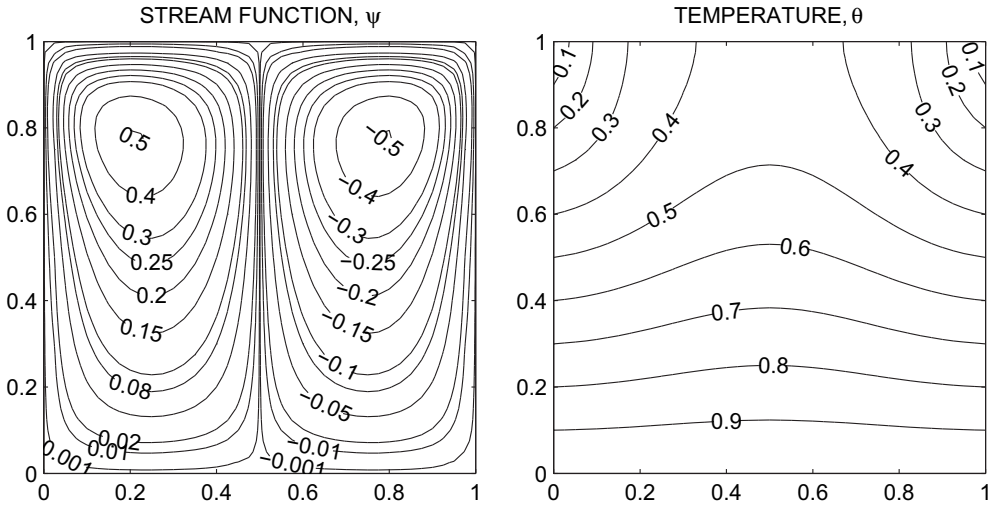

Fig. 4. Contour plots of $\theta(0, Y) = \theta(1, Y) = 1 - Y$ for $Ha = 50$ and $\phi = 0$ ($Pr = 0.025$ and $Ra = 10^5$).

in the upward vertical direction. This process continues as the strength of the magnetic field increases until the four lower cells merge with the two primary recirculating eddies initially positioned in the upper part of the enclosure close to the insulated wall for $Ha = 50$ (Fig. 4). Moreover, vertical stretching of the two cells takes place such that the eyes of the cells get closer to the adiabatic wall. This is accompanied with significant reduction in the fluid movement in the cavity. The braking effect of the magnetic field is observed from the maximum intensity of circulation ψ_{max}. The value of ψ_{max} for $Ha = 0$ is 4.65 while it is equal to 2.52 and 0.50 for $Ha = 20$ and 50, respectively. Temperature stratification becomes dominant as the strength of the magnetic field increases and temperature contour maps tend to become more horizontally uniform in the core region of the enclosure as Ha increases to 50 indicating the approach to a quasi-conduction regime. In addition, the magnetic field is seen to suppress the overall heat transfer in the enclosure. This suppression of convective flows by the use of magnetic fields has proven to be effective in controlling melts and has now been widely practiced in the metals semiconductor crystal growth industries (see, for instance, Series and Hurle [6]). All of the above discussed behaviors are clearly seen in Figs. 2–4.

Figs. 5 and 6 illustrate the influence of the Hartmann number Ha on the streamline and isotherm contours when the magnetic field is applied in the direction normal to the horizontal walls of the enclosure ($\phi = \pi/2$) under the same conditions as Figs. 2–4. Contrary to the behavior of Figs. 2–4 discussed above, it is observed that the two upper primary cells tend to stretch downward as Ha increases. From Fig. 5 for $Ha = 20$, it is seen that the symmetry cells at lower center becomes two small symmetry eddies and the braking effect is less on the two primary upper cells and more on the lower cells than what was observed in Fig. 3. As Ha is increased to 50 in Fig. 6, the two primary cells stretch further down squeezing the four lower cells which are significantly reduced in strength becoming secondary cells to the lower left and right corners of the cavity. As in the case of $\phi = 0$, the temperature of the fluid in the cavity decreases as a results of the application of the magnetic field. However, the level of non-uniformity in the isotherms is higher than the cases observed in Fig. 4. In Fig. 6, the temperature contours are smooth curves which span the entire enclosure and they are generally symmetric with respect to the vertical symmetric line. Unlike Fig. 4 in which the isotherms close to the uniformly heated wall become almost uniform indicating quasi-conduction regime, it

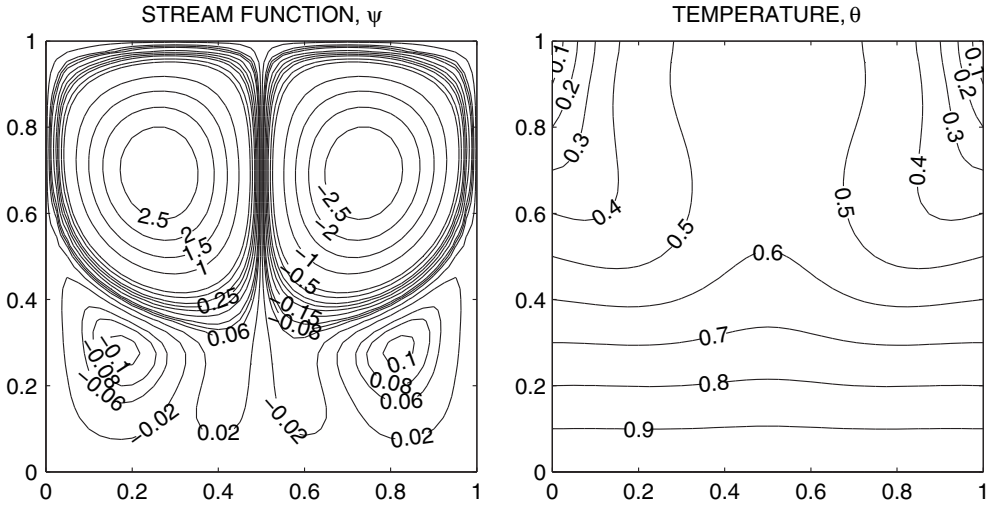

Fig. 5. Contour plots of $\theta(0, Y) = \theta(1, Y) = 1 - Y$ for $Ha = 10$ and $\phi = \pi/2$ ($Pr = 0.025$ and $Ra = 10^5$).

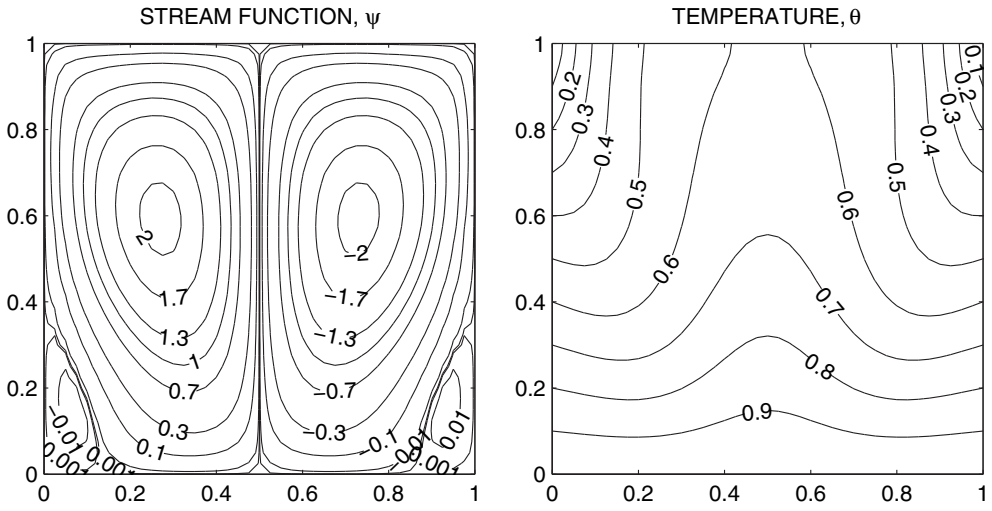

Fig. 6. Contour plots of $\theta(0, Y) = \theta(1, Y) = 1 - Y$ for $Ha = 50$ and $\phi = \pi/2$ ($Pr = 0.025$ and $Ra = 10^5$).

is observed in Fig. 6 that even for relatively high Hartmann number $Ha = 50$, the convection regime is still dominant. This is due to the less flow retardation effect caused by the vertically-applied magnetic field than the horizontally-applied one.

4.1.2. Case II: linearly heated left wall with cooled right wall

Figs. 7–9 depict the effects of the Hartmann number Ha for horizontally-applied ($\phi = 0$) and vertically-applied ($\phi = \pi/2$) magnetic fields on the contour maps of streamlines and isotherms for the case of linearly heated left wall with cooled right wall and uniformly heated bottom wall of the enclosure. From Fig. 7 for $Ha = 0$, it is predicted that due to linearly heated left wall, the fluid rises up along the side of left wall and flows down along the cooled right wall and forms rotating concentric circles in the cavity with center at center of the cavity. At all corners of cavity, secondary circulating cell are formed due to thermal buoyancy effects. The isotherms change their value smoothly from the hot vertical wall to the cold vertical wall with the constant-temperature lines of $\theta > 0.4$ cover around 50% of the cavity. From Fig. 8, as the Hartmann number increases to 50, the movement of the fluid in the cavity slows down, the primary cell and the secondary circulation at left top corner tend to be stretched downward towards the bottom heated wall and the temperature stratification becomes dominant. As evident from Fig. 8, further significant increase in the value of Ha ($Ha = 50$) causes the decrease in the circulation intensity of the primary and secondary cell with increased stretching effect towards the bottom wall. This is represented by the movement of the core or eye of the primary cell downward closer to the uniformly heated bottom wall of the cavity. Fig. 9 shows for $Ha = 50$ and $\phi = \pi/2$, the secondary cell stretches along the linearly heated left wall without losing strength whereas the intensity of the primary cell decreases considerably. In this case, the two cells are considered as primary cells with some difference in movement strength rotating in opposite directions.

4.2. Heat transfer rates: local and average Nusselt number

4.2.1. Case I: linearly heated side walls

Fig. 10a illustrates the effects of the Hartmann number Ha and the magnetic field inclination angle ϕ on the variation of the local Nusselt number at the bottom wall of the cavity Nu_b with the horizontal distance X for the case of linearly heated side walls. At the edges of the bottom wall ($X = 0$ and $X = 1$), $Nu_b = 1$. This is

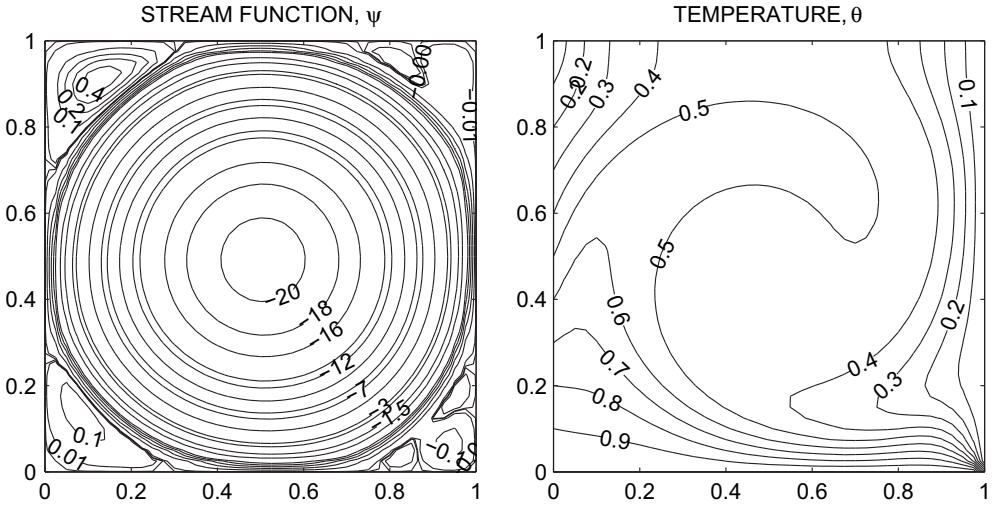

Fig. 7. Contour plots for of $\theta(0, Y) = 1 - Y$ and $\theta(1, Y) = 0$ for $Ha = 0$ ($Pr = 0.025$ and $Ra = 10^5$).

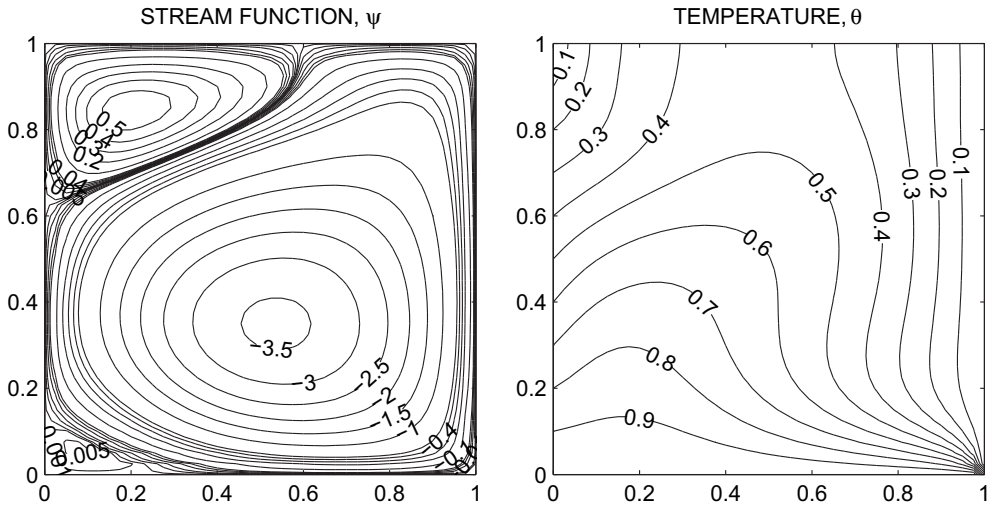

Fig. 8. Contour plots of $\theta(0, Y) = 1 - Y$ and $\theta(1, Y) = 0$ for $Ha = 50$ and $\phi = 0$ ($Pr = 0.025$ and $Ra = 10^5$).

expected due to the linearly heated side walls. In general, it is clearly observed that the local Nusselt number at the bottom wall Nu_b exhibits an oscillatory behavior with the horizontal distance X and that it is exactly symmetric about the centerline of the bottom wall for all values of Ha and ϕ appearing in the figure. This is associated with the symmetry in the thermal boundary conditions of the side walls of the cavity and in the resulting symmetric flow circulation about the centerline of the bottom discussed earlier. It is also observed that for relatively small Hartmann numbers ($Ha = 20$), the rate of heat transfer for a horizontally-applied magnetic field ($\phi = 0$) is higher than its corresponding value for vertically-applied magnetic field $\phi = \pi/2$ in the range $0.2 \leq X \leq 0.8$ with the minimum values occurring at the centerline ($X = 0.5$). However, for higher value of $Ha = 50$, the Nusselt numbers for $\phi = \pi/2$ are considerably higher than their corresponding values for $\phi = 0$. In addition for $Ha = 50$ and $\phi = 0$, the value of Nu_b along the bottom wall is close to unity which indicates the approach to a quasi-conduction regime.

Fig. 10b depicts the variation of the local Nusselt number at the linearly heated side wall of the cavity Nu_s with the vertical distance Y for various values of Ha and ϕ. In general, the values of Nu_s increase as the vertical distance Y increases reaching maximum at $Y = 1$. It is observed that in the upper part of the side wall, the values of Nu_s for $\phi = \pi/2$ are higher than those for $\phi = 0$. However, the opposite is true in the lower part of the side wall. Also, for $Ha = 20$, the distributions of Nu_s along the vertical distance Y for $\phi = 0$ and $\phi = \pi/2$ tend to oscillate close to lower end of the vertical side wall and continues with an increasing trend in its upper end. This behavior is believed to be related the multi-cellular feature represented by the presence of two pairs of symmetric cells with clockwise and counter-clockwise rotations.

Fig. 11 presents the influence of the Hartmann number Ha and the magnetic field inclination angle ϕ on the average Nusselt numbers for the bottom (a) and side wall (b) for the case of linearly heated side walls. It is observed from Fig. 11a and b that for horizontally-applied magnetic field ($\phi = 0$) the average Nusselt numbers for the bottom and side walls decrease significantly as Ha increases up to $Ha = 40$ and then increases slightly as Ha is increased beyond $Ha = 40$. On the other hand, for vertically-applied magnetic field ($\phi = \pi/2$) the average Nusselt numbers exhibit an oscillatory behavior for $0 < Ha < 60$ and they decrease as Ha increases at a faster rate for $60 < Ha < 80$ until they almost level off

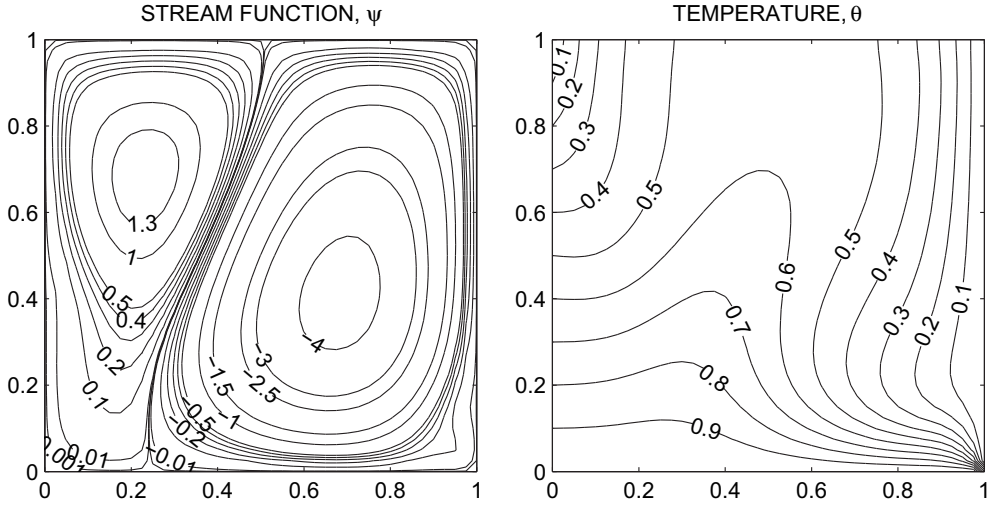

Fig. 9. Contour plots of $\theta(0, Y) = 1 - Y$ and $\theta(1, Y) = 0$ for $Ha = 50$ and $\phi = \pi/2$ ($Pr = 0.025$ and $Ra = 10^5$).

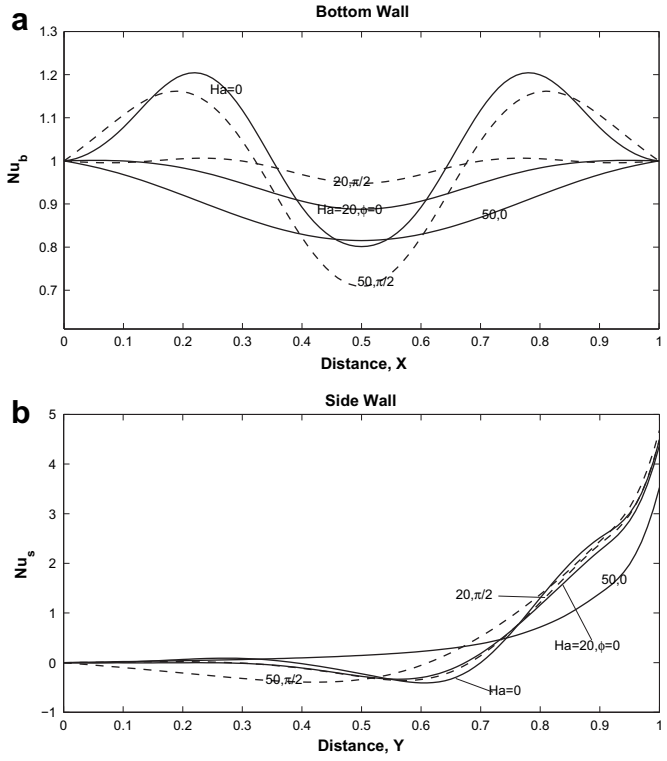

Fig. 10. Variation of local Nusselt number with distance at (a) bottom wall (b) side wall for linearly heated side walls ($Pr = 0.025$ and $Ra = 10^5$).

for $Ha > 80$. In the range $10 < Ha < 70$, the average Nusselt numbers for the bottom and side walls are higher for $\phi = \pi/2$ than for $\phi = 0$. The opposite is true in the ranges $0 < Ha < 10$ and $Ha > 70$.

4.2.2. Case II: linearly heated left wall with cooled right wall

Fig. 12 display the effects of Ha and ϕ on the local Nusselt numbers at the bottom, left and right walls (Nu_b, Nu_l and Nu_r) for linearly heated left wall and cooled right wall, respectively. Fig. 12a shows, in general, that the local Nusselt number Nu_b shows an increasing trend with the horizontal distance X starting from 0 at

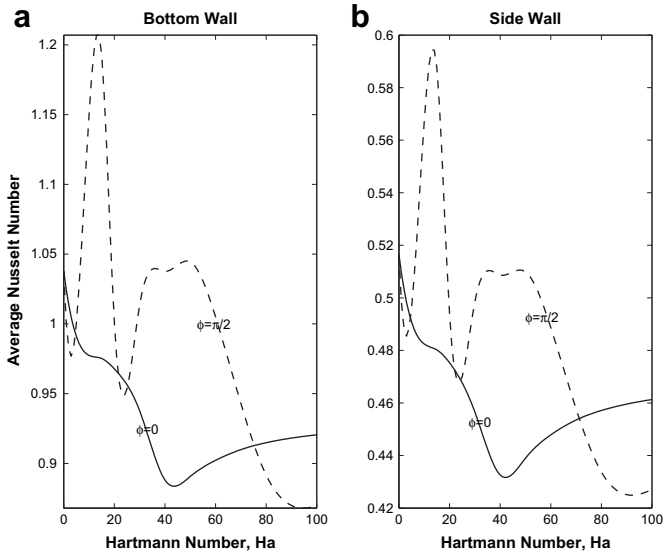

Fig. 11. Variation of average Nusselt number with Hartmann number Ha for linearly heated side walls ($Pr = 0.025$ and $Ra = 10^5$).

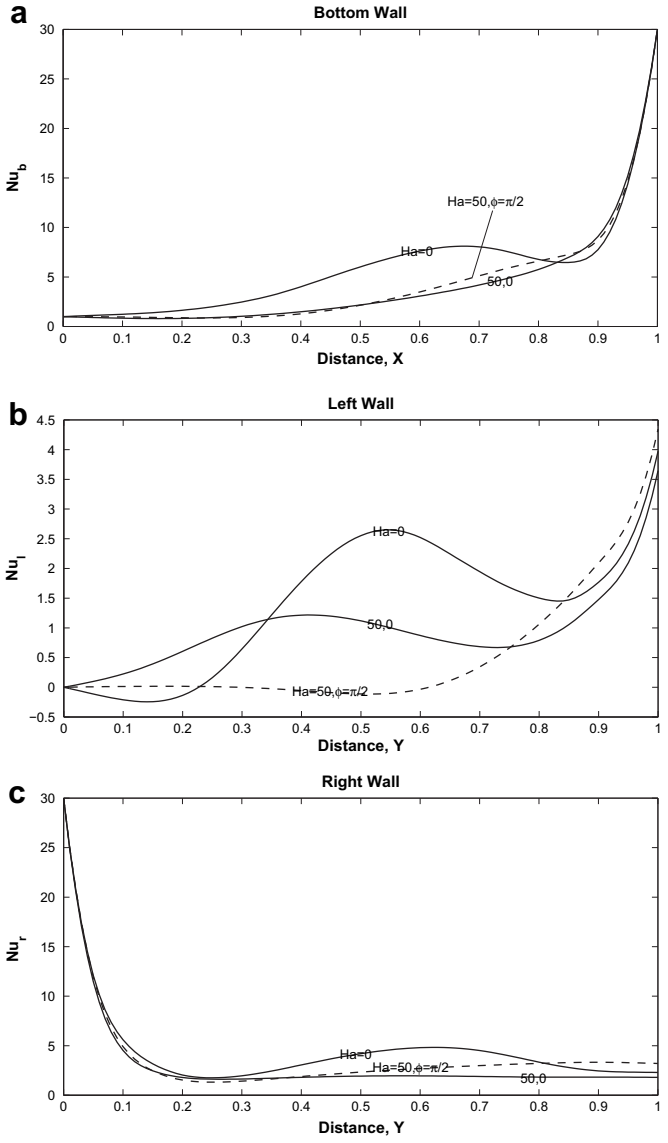

Fig. 12. Variation of local Nusselt number with distance at (a) bottom wall (b) left wall (c) right wall for linearly heated left wall and cooled right wall ($Pr = 0.025$ and $Ra = 10^5$).

the left-edge of the bottom wall due to the linearly heated left wall and becoming maximum at the right-edge of the bottom wall due to the cooled right wall. Away from the walls and as Ha increases, the heat transfer rate decreases. For $Ha = 50$, the values of Nu_b are almost the same for both $\phi = 0$ and $\phi = \pi/2$. Fig. 12b shows the oscillatory trend of Nu_l with increasing values of the vertical distance Y for $Ha = 0$, $Ha = 50$ and $\phi = 0$. However, for $Ha = 50$ and $\phi = \pi/2$, the heat transfer rate becomes negative in the lower part of the left wall without oscillation. As ϕ is increased from 0 to $\pi/2$ for $Ha = 50$, the values of the Nu_l decrease in the lower 75% of the left wall while they increase in its remaining 25%. In Fig. 12c, it is observed that, in general, the value of Nu_r is maximum at $Y = 0$ and decreases as Y increases reaching a minimum at a specific distance in the lower part of the right cooled wall then increases reaching a constant value close to $Y = 1$.

Finally, Fig. 13 elucidates the influence of increasing Ha and ϕ on the average Nusselt numbers for the bottom, left and right walls for the case of linearly heated left wall and cooled right wall, respectively. It is predicted that the average Nusselt numbers for the

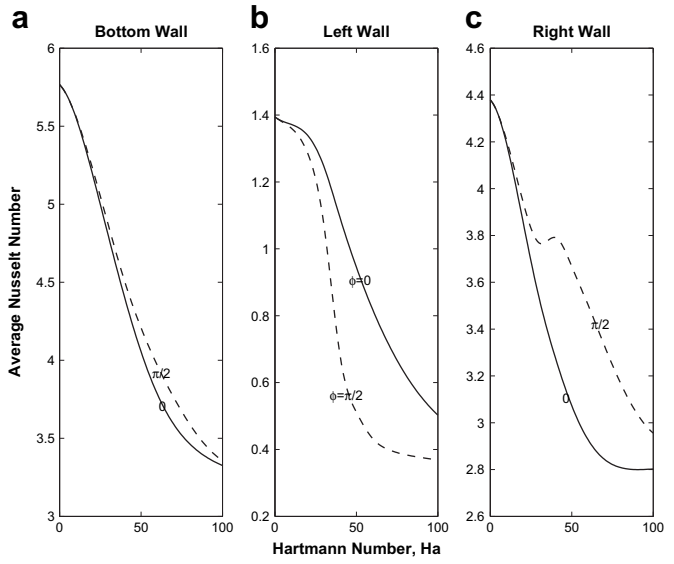

Fig. 13. Variation of average Nusselt number with Hartmann number *Ha* for linearly heated left wall and cooled right wall ($Pr = 0.025$ and $Ra = 10^5$).

bottom, left and right walls decrease as *Ha* increases. However, a mixed effect is shown as ϕ increases. In general, it is observed that the average Nusselt number for the bottom and right walls increase while the average Nusselt number for the left heated wall decreases as ϕ increases.

5. Conclusions

The present study considered steady, laminar, two-dimensional MHD natural convection within a liquid gallium filled square enclosure in the presence of inclined magnetic field for different thermal boundary conditions. The governing equations are developed and the solved by the penalty finite element method with bi-quadratic rectangular elements for the cases of linearly heated side walls and linearly heated left wall with cooled right wall. In both cases, the bottom wall of the enclosure was heated uniformly while the upper wall was kept insulated. It was found that for the case of linearly heated side walls, a multi-cellular (one or three pair) symmetric streamline behavior was predicted for both horizontally-applied and vertically-applied magnetic fields. However, for the case of linearly heated left wall with cooled right wall, a two-cell (one primary and one secondary) feature was predicted. In general, the application of the magnetic field reduces the convective heat transfer rate in the cavity for any inclined angle. In addition, the local Nusselt number at the bottom wall of the cavity exhibited oscillatory behavior along the horizontal distance for the case of linearly heated side walls whereas it increased continuously for the case of linearly heated left wall and cooled right wall with the exception of large Hartmann numbers for a vertically-applied magnetic field. The average Nusselt numbers for the bottom and side walls for the case of linearly heated side walls showed an oscillatory behavior with increasing values of the Hartmann numbers especially for a vertically-applied magnetic field whereas the average Nusselt numbers for the bottom, left and right walls for the case of linearly heated left wall and cooled right wall decreased as the Hartmann number was increased. In general, the average Nusselt number of the uniformly heated bottom wall was higher for vertically-applied magnetic field than for horizontally-applied magnetic field for moderate values of Hartmann numbers for both cases of thermal boundary conditions considered in the present study.

Acknowledgement

The first author wishes to thank the Management of SSN College of Engineering for providing the necessary facility to carry out the present work.

References

[1] K.T. Yang, Natural convection in enclosures. in: S. Kakac, R.K. Shah, W. Aung (Eds.), Handbook of Single-Phase Convective Heat Transfer. Wiley, New York, 1987.
[2] F.A. Kulacki, J.H. Davidson, P.F. Dunn, Convective heat transfer with electric and magnetic field. in: S. Kakac, R.K. Shah, W. Aung (Eds.), Handbook of Single-Phase Convective Heat Transfer. Wiley, New York, 1987.
[3] M. Moreau, Magnetohydrodynamics. Kluwer Acadamic Publishers, The Netherlands, 1990.
[4] H.P. Utech, M.C. Flemmings, Elimination of solute banding in indium antimonide crystals by growth in a magnetic field. Journal of Applied Physics 37 (1966) 2021–2024.
[5] C. Vives, C. Perry, Effects of magnetically damped convection during the controlled solidification of metals and alloys. International Journal of Heat and Mass Transfer 30 (1987) 479–496.
[6] R.W. Series, D.T.J. Hurle, The use of magnetic fields in semiconductor crystal growth. Journal of Crystal Growth 133 (1991) 305–328.
[7] H. Ozoe, E. Maruo, Magnetic and gravitational natural convection of melted silicon – two-dimensional numerical computations for the rate of heat transfer. JSME 30 (1987) 774–784.
[8] H. Ozoe, K. Okada, The effect of the direction of the external magnetic field on the three-dimensional natural convection flow in a cubical enclosure. International Journal of Heat and Mass Transfer 32 (1989) 1939–1954.
[9] J.P. Garandet, T. Albousseiere, M. Moreau, Buoyancy driven convection in a rectangular enclosure with a transverse magnetic field. International Journal of Heat and Mass Transfer 35 (1992) 741–748.
[10] M. Venkatachalappa, C.K. Subbaraya, Natural convection in a rectangular enclosure in the presence of magnetic field with uniform heat flux from side walls. Acta Mechanica 96 (1993) 13–26.
[11] N. Rudraiah, R.M. Barron, M. Venkatachalappa, C.K. Subbaraya, Effect of magnetic field on free convection in a rectangular enclosure. International Journal of Engineering Science 33 (1995) 1075–1084.
[12] S. Alchaar, P. Vasseur, E. Bilgen, Natural convection heat transfer in a rectangular enclosure with transverse magnetic field. Journal of Heat Transfer – Transactions of the ASME 117 (1995) 668–673.
[13] M.C. Ece, E. Buyuk, Natural convection flow under magnetic field in an inclined rectangular enclosure heated and cooled on adjacent walls. Fluid Dynamics Research 38 (2006) 564–590.
[14] S. Mahmud, R.A. Fraser, Magnetohydrodynamic free convection and entropy generation in a square cavity. International Journal of Heat and Mass Transfer 47 (2004) 3245–3256.
[15] T. Grosan, C. Revnic, I. Pop, D.B. Ingham, Magnetic field and internal heat generation effects on the free natural convection in a rectangular cavity filled with porous medium. International Journal of Heat and Mass Transfer 52 (2009) 1525–1533.
[16] I.E. Sarris, I. Lekakis, N.S. Vlachos, Natural convection in a 2D enclosure with sinusoidal upper wall temperature. Numerical Heat Transfer: Part-A 42 (2002) 513–530.
[17] S. Roy, T. Basak, Finite element analysis of natural convection flows in a square cavity with non-uniformly heated wall(s). International Journal of Engineering Science 43 (2005) 668–680.
[18] T. Basak, S. Roy, A.R. Balakrishnan, Effects of thermal boundary conditions on natural convection flows within a square cavity. International Journal of Heat and Mass Transfer 49 (2006) 4525–4535.
[19] E. Bilgen, R. Ben Yedder, Natural convection in enclosure with heating and cooling by sinusoidal temperature on one side. International Journal of Heat and Mass Transfer 50 (2007) 139–150.
[20] M. Sathiyamoorthy, T. Basak, S. Roy, I. Pop, Steady natural convection flows in a square cavity with linearly heated side wall(s). International Journal of Heat and Mass Transfer 50 (2007) 766–775.
[21] B. Sreenivasan, P.A. Davidson, J. Etay, On the control of surface waves by a vertical magnetic field. Physics of Fluids 17 (2005) 117101.
[22] J.N. Reddy, D.K. Gartling, The Finite Element Method in Heat Transfer and Fluid Dynamics. CRC-Press, Florida, 1994.
[23] G.K. Batchelor, An Introduction to Fluid Dynamics. Cambridge University Press, 1993.
[24] G.D. Mallinson, G.D. Vahl Davis, Three-dimensional natural convection in a box: a numerical study. Journal of Fluid Mechanics 83 (1977) 1–31.

Nomenclature

$\overline{B}$: applied magnetic field
B: magnitude of magnetic field
g: acceleration due to gravity, m s^{-2}
L: side of the square cavity, m
Nu: local Nusselt number

$\overline{Nu}$: average Nusselt number
Ha: Hartmann number
p: pressure, Pa
P: dimensionless fluid pressure
Pr: Prandtl number
Ra: Rayleigh number
T: fluid temperature, K
T_c: temperature of cold at top edges of side walls, K
T_h: temperature of hot (bottom) wall, K
u: x component of velocity
U: x component of dimensionless velocity
V: y component of velocity
V: y component of dimensionless velocity
X: dimensionless distance along *x* coordinate
Y: dimensionless distance along *y* coordinate

Greek symbols

α: thermal diffusivity, $m^2\ s^{-1}$
β: volume expansion coefficient, K^{-1}
γ: penalty parameter
σ: electrical conductivity, $\Omega^{-1}\ m^{-1}$
θ: dimensionless temperature
ν: kinematic viscosity, $m^2\ s^{-1}$
ρ: density, $kg\ m^{-3}$
ψ: stream function
ϕ: inclined angle

Subscripts

b: bottom wall
c: cooled wall
h: hot wall
l: left wall
r: right wall
s: side wall